

Superconformal Electrodeposition in Submicron Features

D. Josell, D. Wheeler, W. H. Huber, and T. P. Moffat

National Institute of Standards and Technology, Gaithersburg, Maryland 20899

(Received 11 December 2000; published 15 June 2001)

Superconformal electrodeposition is explained based on a local growth velocity that increases with coverage of a catalytic species adsorbed on the copper-electrolyte interface. For dilute concentration of the catalyst precursor in the electrolyte, local coverage in fine features changes more due to interface area change than by accumulation from the electrolyte, yielding superconformal growth. The model is supported by experiments and simulations of copper deposition in 350–100 nm wide features, helping to explain the influence of adsorbates on roughness evolution.

DOI: 10.1103/PhysRevLett.87.016102

Superconformal copper electrodeposition in the Damascene process for microelectronic fabrication represents a significant advance enabling a new generation of integrated circuits. Such “superfilling” of trenches and vias results from more rapid growth at the bottom of the trenches than at the sidewalls. Early modeling studies focused on the location-dependent growth rate derived from diffusion-limited consumption of an inhibiting species [1–3]. However, it was necessary to empirically modify the theory to capture the experimentally observed shape evolution [1,2]. Although the derived constitutive equations provide a reasonable description of feature filling, the required modification undermines the physical basis of the model.

Subsequent research revealed that superconformal deposition in submicron features involves competitive interaction between species that accelerate and inhibit deposition [4–7]. A model system exhibiting the characteristics required for successful on-chip metallization was identified [7]. The electrolyte contained three additives: chloride (Cl), polyethylene glycol (PEG), and 3-mercaptopropanesulfonate (MPSA). Inhibition is provided by the interaction between PEG-Cl and the copper surface, acceleration by competitive adsorption of MPSA, or a derivative. The competitive interaction results in hysteresis of current-voltage (i - η) polarization curves as well as the “overfill” phenomena [7]. The latter term describes the change of the surface profile associated with growth in the trench from concave to convex due to sustained acceleration of the deposition rate after filling is complete. Such overfill cannot be rationalized by the transport-limited inhibition model outlined above [4–7].

This paper presents a model of superconformal deposition where the kinetics and mechanism of the metal deposition reaction are dependent on the fractional surface coverage θ of a catalytic or accelerating species (derived here from MPSA). At a flat planar electrode, accumulation is determined by the concentration C_{MPSA} ($\mu\text{mol/L}$ range) of the bulk electrolyte. In the first approximation the adsorbed species remains on the copper-electrolyte interface during copper deposition without being incorporated into the solid. The coverage θ cannot exceed one monolayer. On nonplanar geometries, such as rough or patterned

PACS numbers: 81.15.Pq, 68.43.Jk, 82.45.Jn, 82.65.+r

surfaces, local θ also changes inversely to changes of a local electrode surface area during growth. Accordingly, the coverage increases during conformal growth on a concave surface while the opposite is true for a convex surface. For superconformal deposition in a given submicron feature, this effect outweighs changes due to accumulation from the electrolyte or loss from incorporation in the growing solid. Surface diffusion of the catalytic species is assumed to be negligible during deposition.

The deposition reaction: obtaining kinetic parameters.—The capacity for the MPSA-derived adsorbates to simultaneously float on the growing surface and accelerate the rate of copper deposition was revealed using slow scan rate voltammetry. Deposition on freshly polished polycrystalline copper electrodes was examined in acidified cupric sulfate solutions containing 88 $\mu\text{mol/L}$ PEG, 1 mmol/L NaCl, and a range of C_{MPSA} . Additional details are published elsewhere [7]. Cyclic i - η curves [Fig. 1(a)] reveal hysteresis that arises from the displacement of the inhibiting PEG-Cl complex by the accumulating MPSA derivative on the surface. The i - η curves are displaced toward positive potentials as C_{MPSA} increases from 0 to 10.2 $\mu\text{mol/L}$. The acceleration characterizing the reverse sweep is maximized at $C_{\text{MPSA}} \approx 5 \mu\text{mol/L}$, indicating saturation of the surface coverage. At high overpotentials the deposition rate is independent of potential due to transport limitations on the cupric ion.

The hysteretic i - η curves are described by the generalized current-overpotential equation that includes the effect of cupric ion depletion at high overpotentials η [volts] [8],

$$i(\theta, \eta) = i_0(\theta) \left(1 - \frac{i}{i_L}\right) \exp\left(-\frac{\alpha(\theta)F}{RT} \eta\right). \quad (1)$$

The exchange current density, $i_0(\theta)$, describes the dynamic exchange that characterizes equilibrium and the transfer coefficient, $\alpha(\theta)$, characterizes the symmetry of the energy barrier for charge transfer. They are both functions of the fractional surface coverage θ of the MPSA-derived accelerator, defined in terms of the maximum coverage $\Gamma = 9.8 \times 10^{-10} \text{ mol/cm}^2$, corresponding to a $\sqrt{3} \times \sqrt{3} R30^\circ$ structure on Cu(111). The transport-limited deposition rate, $i_L \approx 20 \text{ mA/cm}^2$, is determined by boundary

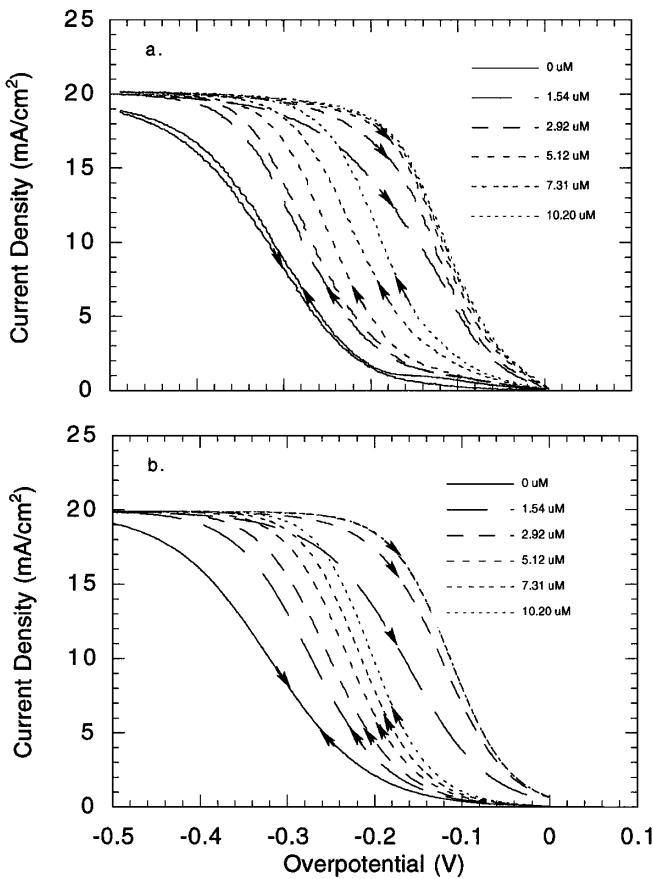


FIG. 1. (a) Slow sweep cyclic voltammograms revealing hysteresis as a function of C_{MPSA} . (b) Simulations of the i - η curves assuming accumulation of a MPSA-derived catalyst. Note abbreviation $\mu\text{M} \equiv \mu\text{mol/L}$.

layer diffusion, free convection, and cupric ion concentration Cu^{2+} . Finally, $F = 96485 \text{ C/mol}$, $R = 8.314 \text{ J/mol K}$, and $T = 293 \text{ K}$.

The time-dependent surface coverage $\theta(t)$ was calculated for C_{MPSA} of each electrolyte using irreversible statistical adsorption at the interface [9,10]

$$\frac{d\theta}{dt} = k^* C_{\text{MPSA}}^i (1 - \theta) \quad (2)$$

with accelerator concentration C_{MPSA}^i in the electrolyte adjacent to the interface. Equating the adsorbing flux to that diffusing from the bulk electrolyte gives

$$k^* C_i (1 - \theta) = \frac{D_{\text{MPSA}}}{\Gamma} \frac{(C_{\text{MPSA}} - C_{\text{MPSA}}^i)}{\delta} \quad (3)$$

for a psuedo-steady-state gradient that relaxes up to a boundary layer thickness $\delta = 135 \mu\text{m}$ with $D_{\text{MPSA}} = 1 \times 10^{-5} \text{ cm}^2/\text{s}$ [10]. Using Eq. (3) to eliminate C_{MPSA}^i , Eq. (2) was numerically integrated to obtain $\theta[t, C_{\text{MPSA}}, k^*(\eta)]$ for the 1 mV/s sweep rate for η from 0 to -0.5 V and back to 0 V. Using this expression for θ in Eq. (1), the functions $k^*(\eta) = 1.8 \times 10^5 - 2.5 \times 10^7 \eta^3 [\text{cm}^3/\text{mol s}]$, $i_0(\theta) = 0.069 + 0.64\theta [\text{mA/cm}^2]$, and $\alpha(\theta) = 0.447 + 0.299\theta$ were determined by fitting

the voltammetric data in Fig. 1(a). The rate constant k^* increases during the negative going sweep; it is held at $k^*(-0.5)$ on the return sweep to model obstruction of the PEG-Cl blocking layer's healing by the adsorbing accelerator [7]. The simulations shown in Fig. 1(b) were obtained with the two parameter $k^*(\eta)$, $i_0(\theta)$, and $\alpha(\theta)$. Whereas one inflected curve through the origin requires at least three parameters to describe it, twelve curves, nine distinct, are being fit here using only seven fitting parameters [i_L plus two each for $k(\eta)$, $i_0(\theta)$, and $\alpha(\theta)$]. The quality of the fit to the experimental curves (rms error is $\approx 0.7 \text{ mA/cm}^2$) supports the accumulation model, especially when one considers that regions of kinetic-limited θ accumulation, diffusion-limited θ accumulation, and diffusion-limited Cu^{2+} arrival are all being modeled in Fig. 1(b). The fits do however, as a fraction, significantly underestimate the experimental current at $|\eta| < 0.2 \text{ V}$ on the outgoing sweeps. Chronoamperometry (current-transient studies at fixed η) is being used to further assess the kinetics under these conditions.

Feature filling: modeling and experiment.—Simulations were performed to explore the effect of compression (dilation) of the adsorbed species during filling of submicron features using $i(\theta, \eta)$ obtained above. The local growth velocity, in terms of the local current, equals $i(\theta, \eta)\Omega_{\text{Cu}}/2F$ (2 for Cu^{2+} ionization and $\Omega_{\text{Cu}} = 7.1 \text{ cm}^3/\text{mol}$). Conservation of MPSA on the interface of the filling feature dictates that Eq. (2) becomes

$$\frac{d\theta}{dt} = \frac{i\Omega_{\text{Cu}}}{2F} \kappa\theta + k^* C_{\text{MPSA}}^i (1 - \theta), \quad (4)$$

where κ is the local curvature of the interface. The κ dependence leads to increasing (decreasing) local coverage on concave (convex) surfaces during growth. *This term dominates at the bottom of superfilling features.*

The interface evolution was modeled using the level-set method with a finite difference scheme to solve the diffusion equations for Cu^{2+} and MPSA on a regular grid. The parameters are as above with $D_{\text{Cu}^{2+}} = 5.6 \times 10^{-6} \text{ cm}^2/\text{s}$. In the calculations, the ratio of cupric ion concentrations at the interface versus the bulk, $1 - i/i_L$ in Eq. (1) for flat specimens, was evaluated locally from the Cu^{2+} concentration profile. The patterned trenches were $\approx 0.46 \mu\text{m}$ deep, $\approx 0.56 \mu\text{m}$ with the Cu seed. A depth of $0.5 \mu\text{m}$ was used for the calculations. Modeled aspect ratios of 5.6, 4.0, and 3.0 equal $0.56 \mu\text{m}$ divided by the widths of the three narrowest trenches examined experimentally. The ≈ 6 and $\approx 10 \text{ nm}$ thick Cu seeds on the sidewalls and bottoms of the trenches, respectively, were ignored. The simulations (Fig. 2) show behavior that depends on C_{MPSA} , overpotential, and trench aspect ratio.

One must typically model the spacing as well as the dimensions of the features as concentrations will drop more across the convecting boundary layer due to the added consumption on the sidewalls of the closely packed trenches. This is important when the MPSA is at the crossover

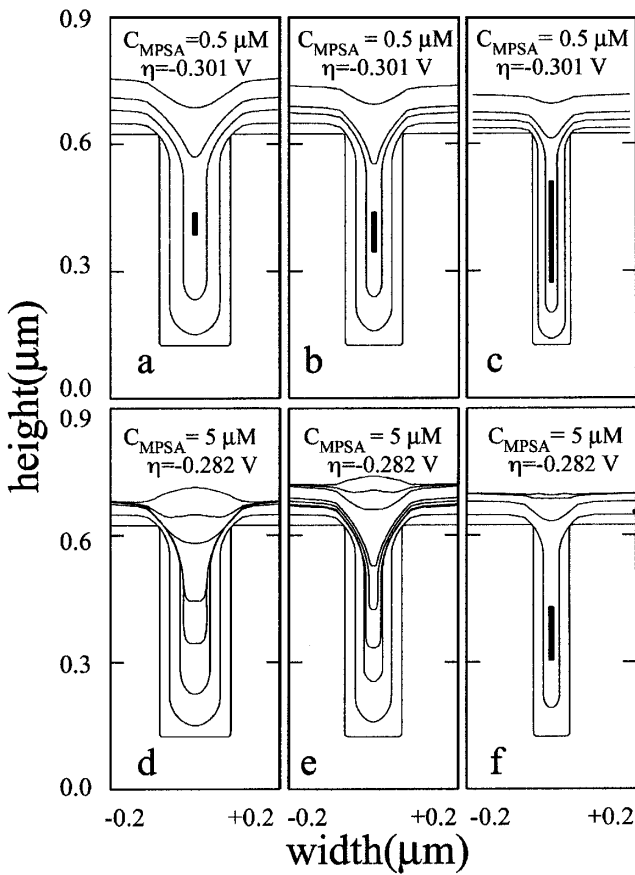


FIG. 2. Simulations of copper deposition in trenches with aspect ratios of 3.0, 4.0, and 5.6 (left to right) for indicated C_{MPSA} and η . Note abbreviation $\mu\text{M} \equiv \mu\text{mol/L}$.

between kinetically controlled versus diffusion-limited absorption; the effect on C_{MPSA}^i can be approximately obtained if one scales k^* in Eqs. (2) and (3) by the actual surface area divided by that for a flat substrate. Here, because only a $50 \mu\text{m} \times 50 \mu\text{m}$ region of each 1 cm^2 specimen is patterned, the concentrations are taken to be those for flat substrates. Trenches were therefore modeled as $5 \mu\text{m}$ apart (nearly isolated) rather than their experimental $0.5 \mu\text{m}$ spacing. The $\approx 10\%$ increase of area due to the sidewalls reduces C_{MPSA}^i midway between trenches $\approx 10\%$ below that over a flat substrate in the modeled results. The rate of accumulation, most affected at low θ [see Eq. (4)], is similarly reduced.

Superfilling is seen in Figs. 2(d) and 2(e). Consistent with observations, growth is initially conformal because the catalytic species needs time to accumulate and concentrate. Under optimal conditions, θ and the velocity of the bottom quickly increase, resulting in rapidly accelerating upward growth with minimal sidewall motion. The value of θ is not permitted to exceed 1; additional material is deleted (deactivated). As the growth front approaches the top of the trench, its curvature changes sign, forming the bumps visible above the trenches. If the aspect ratio of the trench is too great, the sidewalls impinge at the

top of the trench before the bottom surface can escape, typically forming a void in the trench and a cusp above it [Figs. 2(a)–2(c), 2(f)].

The model predictions, with all kinetic parameters from the i - η measurements, were compared with filling experiments. Copper was electroplated in patterned trenches under different deposition conditions. The trench widths varied from 350 to 100 nm with aspect ratios from 1.5 to 4.6 (without Cu seed). Copper was deposited at fixed voltage, with the overpotentials η corresponding to $\sim 10 \text{ mA/cm}^2$ on the appropriate negative-going i - η curve (Fig. 1). Further experimental details can be found elsewhere [7]. Deposition from an additive-free cupric sulfate solution yields voids in all the trenches along with the cusped surface profile anticipated for conformal deposition [Fig. 3(a)]. For $C_{\text{MPSA}} = 0.5 \mu\text{mol/L}$ ($\eta = -0.301 \text{ V}$) voids are apparent in the two finest features [Fig. 3(b)]. The model predicts voids in the three finest features [Figs. 2(a)–2(c)]. For $C_{\text{MPSA}} = 5 \mu\text{mol/L}$ ($\eta = -0.282 \text{ V}$) all features are filled [Fig. 3(c)]. Bumps, consistent with superfilling, are visible over all but the finest feature; it is unclear if this feature contains a seam. The model predicts superfilling for all but the finest feature [Figs. 2(d)–2(f)]. For $C_{\text{MPSA}} = 40 \mu\text{mol/L}$ ($\eta = -0.150 \text{ V}$) voids appear in all trenches with an aspect

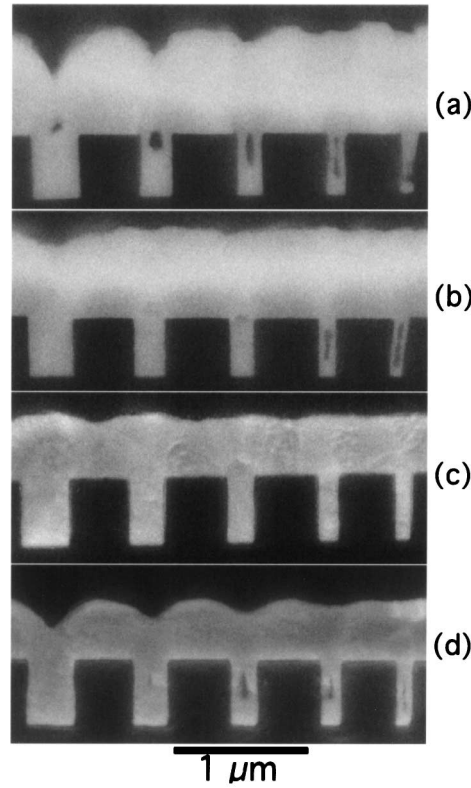


FIG. 3. Scanning electron microscope images of trenches filled from electrolytes with C_{MPSA} : 0, 0.5, 5, and $40 \mu\text{mol/L}$, and overpotentials η : -0.097 , -0.301 , -0.282 , and -0.150 mV (top to bottom), and aspect ratios (without Cu seed): 1.5, 1.9, 2.5, 3.3, and 4.6 (left to right).

ratio greater than 1.5 [Fig. 3(d)]. The grooved surface profile indicates that the system has reverted toward conformal growth.

The experimentally observed dependence of trench filling on C_{MPSA} is understood within the model. In too dilute solutions ($C_{\text{MPSA}} \approx 0.5 \mu\text{mol/L}$), coverage θ is so low that the geometrically driven enrichment yields insufficient acceleration for bottom-up filling. In overly concentrated solutions ($C_{\text{MPSA}} \approx 40 \mu\text{mol/L}$), the surface coverage everywhere increases rapidly toward saturation, giving conformal growth. Superfilling is obtained for near-optimum concentrations ($C_{\text{MPSA}} \approx 5 \mu\text{mol/L}$).

Future studies should consider consumption and/or desorption of the catalyst to maintain unity coverage on the saturated bottom surface. Desorption will accelerate sidewall coverage and growth rates, without affecting the velocity of the bottom surface; this will restrict the range of conditions for which superfill can occur.

In summary, a simple catalyst mediated deposition model has been shown to quantitatively predict three experimental observations relevant to superfilling submicron features in Damascene processing, namely, (1) an initial period of conformal growth, (2) subsequent accelerated growth from the bottom of the trench, and (3) final inversion of the growth front giving overfill bumps. Modeling of voltammetric i - η hysteresis was used to quantify the rate of catalyst adsorption and its effect on the deposition rate of copper. The derived parameters were used in the catalyst mediated deposition model. This shape-change model was then used to predict fill patterns, thus determining the conditions under which superconformal deposition occurs. The model developed here has general

implications for understanding the use of organic additives to produce smooth “bright” surfaces by electrodeposition, and is distinct from models based on diffusion-limited accumulation of inhibiting molecules.

-
- [1] P. C. Andricacos, C. Uzoh, J. O. Dukovic, J. Horkans, and H. Deligianni, IBM J. Res. Dev. **42**, 567 (1998).
 - [2] H. Deligianni, J. O. Dukovic, P. C. Andricacos, and E. G. Walton, in *Proceedings of the International Symposium on Electrochemical Processing in ULSI Fabrication and Semiconductor/Metal Deposition II*, edited by P. C. Andricacos *et al.* (Electrochemical Society Inc., Pennington, NJ, 2000), Vol. 99-9, p. 52.
 - [3] A. C. West, J. Electrochem. Soc. **147**, 227 (2000).
 - [4] J. Reid and S. Mayer, in *Proceedings of the Advanced Metallization Conference, 1999*, edited by M. E. Gross, T. Gessner, N. Kobayashi, and Y. Yasuda (MRS, Warrendale, PA, 2000), p. 53.
 - [5] T. Ritzdorf, D. Fulton, and L. Chen, in *Proceedings of the Advanced Metallization Conference, 1999* (Ref. [4]), p. 101.
 - [6] E. Richard *et al.*, in *Proceedings of the Advanced Metallization Conference, 1999* (Ref. [4]), p. 149.
 - [7] T. P. Moffat *et al.*, J. Electrochem. Soc. **147**, 4524 (2000).
 - [8] A. J. Bard and L. R. Faulkner, *Electrochemical Methods, Fundamental and Applications* (Wiley, New York, 1980).
 - [9] O. Dannenberger, M. Buck, and M. Grunze, J. Phys. Chem. B **103**, 2202 (1999).
 - [10] L. S. Jung and C. T. Campbell, Phys. Rev. Lett. **84**, 5164 (2000).